Estimation of nn scattering rates from colliding laser-induced TNSA or ICF neutrons

Mark Yuly, Avery Belanger.

I. Motivation

Modern high-power short-pulse lasers may make it possible to measure neutron-neutron scattering, a long sought-after goal in nuclear physics which has proven elusive due to difficulty producing the required neutron densities. By making use of the high density of primary neutrons produced in inertial confinement fusion (ICF) or by neutron-producing reactions generated by ions accelerated via target normal sheath acceleration (TNSA), a neutron scattering measurement may be possible in the near future. This idea was suggested [1] as one of the flagship experiments for the proposed NSF-OPAL laser system, but because this experiment required significant advances before it could be implemented the decision was ultimately made to wait. According to the *OPAL Flagship Experiment Selection Report* [2]

> "The proposal stated a clear, strong scientific goal. It lays out a reasonable path to achieving with target and detector development efforts, as well as preparatory experiments that could be performed at other facilities. The "future flagship" experiment would prove extremely challenging. If successful, it would advance nuclear physics strongly and demonstrate the utility of nuclear photonics while also developing ultrafast, pulsed neutron sources that could find other applications."

One of the perceived weaknesses of the proposal was the concern "that no codes exist to model these effects and confirm that we could be in the right regime." The in-progress work described in this report is an attempt to address this concern.

The quantity ultimately of interest in low-energy nucleon-nucleon scattering is the so-called "scattering length", denoted by the letter a. The strong-nuclear component of the nucleon-nucleon elastic scattering cross section can be expanded into partial waves. At low energy, the higher angular momentum terms can be neglected and only the s-wave ($\ell = 0$) term retained. If the strong nuclear potential is assumed to have a well-defined edge, then matching the boundary conditions with the s-wave wavefunction yields an approximate solution for the singlet ($S = 0$) cross section.

However, when the nucleons are unpolarized, there are four possible spin states: $S = 1$, $s_z = -1, 0, 1$ (triplet) and $S = 0, s_z = 0$ (singlet). This means the cross section (due to the strong nuclear potential) is the weighted average

$$\sigma = \frac{3}{4}\sigma_t + \frac{1}{4}\sigma_s \tag{1}$$

where σ_t and σ_s are the triplet and singlet cross sections respectively. For *np* scattering both singlet and triplet terms are present, but for *pp* and *nn* scattering, since the interacting particles are identical, the triplet spin state is not allowed by the exclusion principle. In the case of *pp* scattering there is the additional complication that both protons are electrically charged, so the experimentally measured cross section involves both electromagnetic and strong nuclear interactions from which the pure nuclear interactions must be extracted using theory.

It can be shown (c.f. Ref. [3]) that the cross section for low-energy *nn* scattering in the center-of-mass frame should be approximately

$$\sigma(k) = \frac{1}{4}\sigma_s = \frac{\pi a_{nn}^2}{\left[1 - \frac{1}{2} a_{nn} R_{nn} k^2\right]^2 + a_{nn}^2 k^2} \tag{2}$$

where R_{nn} is the effective range and a_{nn} is the *nn* scattering length, measurement of which is the purpose of the experiment being proposed. The neutrons are scattered isotopically in the CM frame. The wave number k, which is defined to be

$$k = \sqrt{\frac{2\, m_n\, E_{rel}}{\hbar^2}} \tag{3}$$

with neutron mass m_n and relative kinetic energy E_{rel}. As shown in Figure 1, using estimated values for $a_{nn} \approx -18.5$ fm and effective range, $R \approx 2.75$ fm [4], the total *nn* cross section rises rapidly to a maximum value of about $d\sigma/d\Omega_{cm} = a_0^2/4 \approx 0.86$ b/sr.

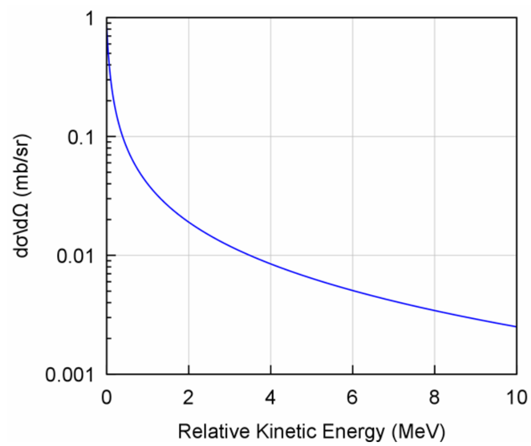

Figure 1. Estimated differential cross section for *nn* scattering in the CM frame as a function of relative kinetic energy.

The reason for so much interest in low-energy neutron-neutron scattering is that such a measurement could provide a powerful test of charge symmetry and charge invariance in the strong nuclear force, and would provide a very sensitive constraint on nuclear potential models. The idea that the strong nuclear force exhibits charge symmetry led directly to the concept of isospin. In this framework, protons and neutrons are considered different isospin states of the same particle, the nucleon, having total isospin $I = 1/2$, with protons having $I_3 = 1/2$ and neutrons $I_3 = -1/2$. Charge symmetry is invariance under the inversion of I_3, that is, changing protons into neutrons and vice versa. As shown in Figure 2, if charge symmetry holds then two protons should have the same strong interaction as two neutrons, hence scattering length $a_{pp} = a_{nn}$. On the other hand, inverting the isospin in a reaction involving a neutron and a proton would just give a neutron and proton back again, so charge symmetry does not give any insight into the strong *np* interaction or the singlet *np* scattering length a_{np}. Charge independence, also called isospin symmetry, however, means the strong force is completely invariant under *any* rotation in isospin space, leading to the conclusion that protons and neutrons would interact exactly the same via the strong force, and hence that $a_{pp} = a_{nn} = a_{np}$.

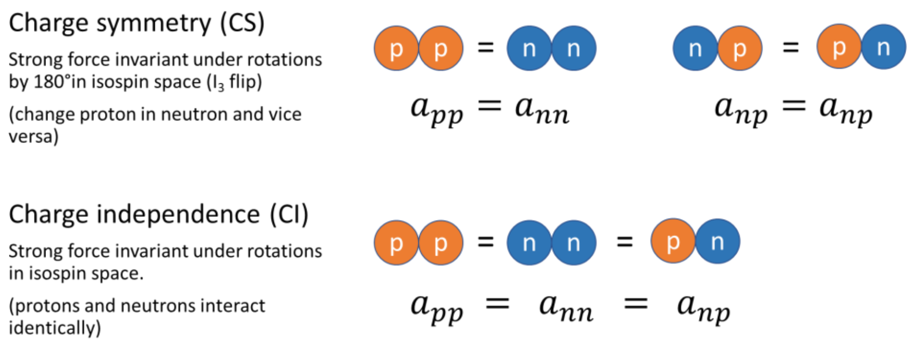

Figure 2. Charge symmetry means the strong interaction is invariant under inversion of I_3, meaning *nn* and *pp* interactions would be the same, but saying nothing about *np* interactions. Charge independence would be if the strong force was invariant under any isospin rotation, which would mean that the *np* interaction was also the same as *nn* and *pp*.

Because experimentally it is easy to create a proton target, and because there is no coulomb interaction, previous measurements of a_{np} are quite precise. On the other hand, measurements of a_{pp} have a much larger uncertainty, mostly due to the theory problem of extracting the nuclear scattering length from measured cross sections that include coulomb repulsion. Figure 3 compares the measured values of a_{pp} and a_{np} with measurements of a_{nn}. The *nn* scattering length is very difficult to measure because of the unavailability of a high-density neutron target. In practice, this means measurements must be made using deuteron targets, and the effect of the proton on the neutron-neutron scattering has to be accounted for using theory. From Figure 3 it is clear that the values obtained by these techniques for a_{nn} vary widely by type of experiment, by as much as 4σ, and that is why it is difficult to say anything meaningful about charge symmetry from scattering length measurements.

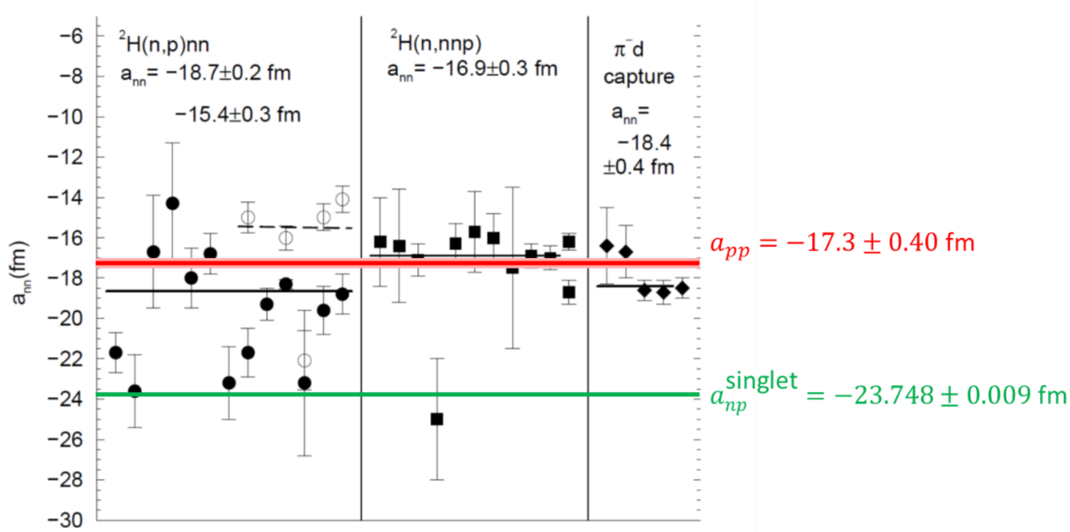

Figure 3. Comparison of values for a_{nn} indirectly extracted from previous measurements (solid dots) of ^{3}H(n,p)nn, ^{2}H(n,nnp), and π^-d. as well as reanalysis of this data using modern techniques (open circles). Measurements for each reaction are roughly chronological from left to right. Also shown are measurements of a_{pp} [5] and a_{np}^{singlet} [6]. Figure modified from Ref. [7].

Moreover, it can be shown [8] that the scattering length is very sensitive to the depth V of the nuclear potential well

$$\frac{\delta a_{nn}}{a_{nn}} = 1.23\frac{a_{nn}}{R_{nn}}\frac{\delta V}{V} \sim 10\frac{\delta V}{V} \quad (4)$$

so that a precise measurement of a_{nn} would provide a useful constraint on the potentials used in nuclear models.

II. Previous Attempts

While there have been several experiment studies or proposals [9, 10], there have only been two serious previous attempts to directly measure the *nn* scattering cross section at low energies. The first experiment [4, 11] was the truly heroic effort, shown on the left in Figure 4, to use the primary 14.1 MeV DT neutrons from two underground thermonuclear explosions. Neutrons were transported down shielded, collimated, evacuated tubes to an evacuated chamber where they could collide. The uncollided neutrons continued down the tubes to TOF detectors used to determine the incident velocity spectra. Surprisingly, the scattered neutrons travel on the surface of a narrow cone centered on the CM velocity, rather than just within the cone; the reason for this unexpected result is explained in Section **VI.C.** The scattered neutrons then traveled down a central tube to two detectors, one containing the cone surface and the other outside, the scattered neutrons and the background to be measured simultaneously.

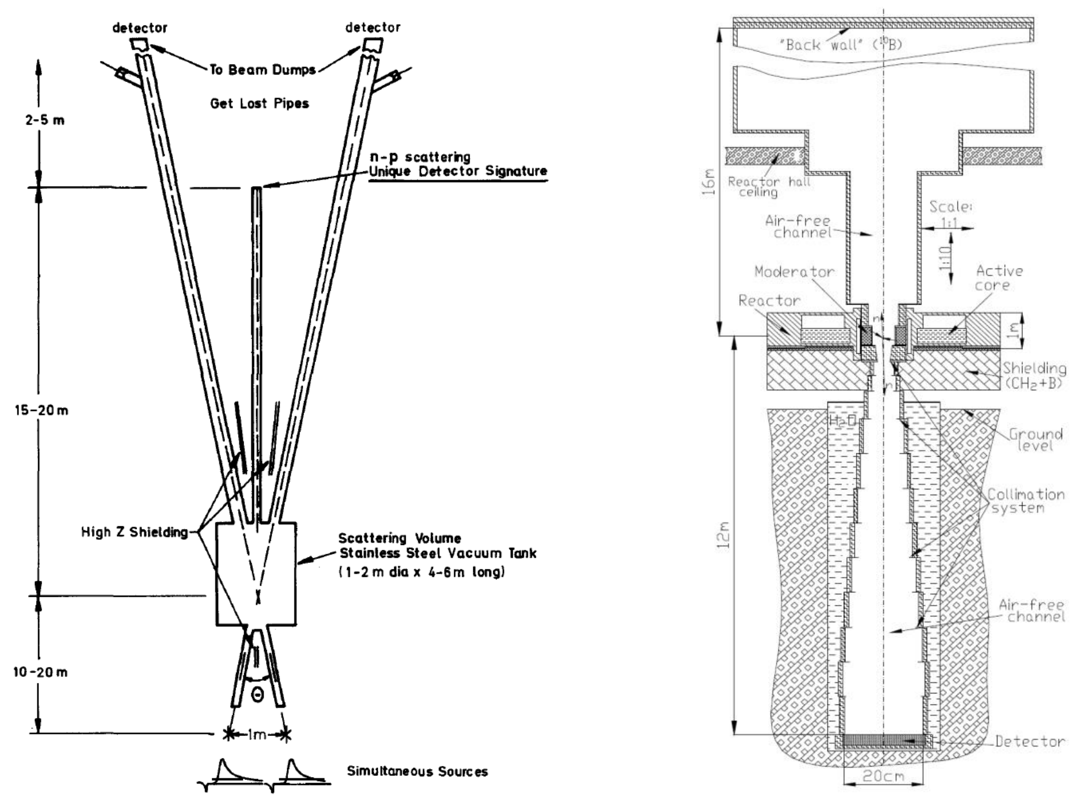

Figure 4. (Left) The Los Alamos neutron-neutron scattering experiment. Figure taken from Ref. [4]. (Right) The YAGUAR Reactor neutron scattering experiment. Figure taken from Ref. [18].

Because of obvious security concerns, it is hard to find much information about the results of this experiment. According to Ref. [4], "A feasibility test was actually performed in April 1986. Neutrons from the simultaneous (within 2 ns) underground explosions of two fission-fusion devices were collimated by 565 tons of copper-iron-lead shielding into two channels intersecting at $\theta = 3.8°$. The collision volume was about 12 cm^3. The scattered neutrons were detected using scintillators and measuring the integral charge from the phototubes." No further information was forthcoming, and, of course, such an experiment quickly became impossible because of the US moratorium on nuclear explosive testing, a policy that has been in place since 1992.

Work on the second *nn* scattering experiment [12-131415161718192021], which used thermal neutrons generated by the YAGUAR aperiodic pulsed reactor in Snezhinsk, Russia, occurred from 2002 to 2012. This reactor produces about 32 MJ of energy in 900-1000 μs long pulses, during which about 10^{18} neutrons are released with average neutron energy of about 0.9 MeV. As sown in Figure 4, at the center of the annular reactor was an evacuated scattering chamber. Neutrons were moderated to thermal energies by a polyethylene ring around the chamber, where they reached densities as high as 10^{13} n/cm^3. Thermal neutrons that scattered off each other in the scattering chamber could have a vertical component of velocity and travel down a 12 m long collimated tube to a specially designed ^{3}He ionization detector. Neutrons scattered in the opposite direction traveled 16 m to the boron coated "back wall" where they are absorbed or reflected back. Careful collimation reduced thermal neutrons that multiply scattered from the walls, and time-of-flight was used to separate fast neutrons coming from the source as well as neutrons reflected from the back wall.

Unfortunately, later tests [21] revealed that there was a sizeable unexpected background due to *np* scattering from desorbed H_2 and H_2O from the stainless-steel walls of the scattering chamber, possibly as a result of the gamma flash from the reactor pulse. Apparently, no solution was found to this problem, and the project was ultimately abandoned.

III. Description of Proposed Experiment

The experiment being proposed is similar to the Los Alamos neutron-neutron scattering experiment, except on the scale of millimeters rather than scores of meters. Consider the scattering geometry for neutrons produced by two laser induced neutron sources, shown in Figure 5. In this diagram, the pulses of neutrons could be produced by two ICF implosions or by two lasers striking two TNSA targets to accelerate ions which then produce neutrons when the strike a target. For TNSA the neutrons have an angular and energy distribution $Y(\theta_n, E_n) \equiv d^2N_n/dE_n d\Omega_n$ and are produced via a particular nuclear reaction, such as 2H(d,n)3He, 3H(d,n)4He, 7Li(p,n)7Be, or 7Li(d,n)8Be. These reactions produce monoenergetic neutrons, but because the TNSA process produces a spread of incident ion energies, the resulting outgoing neutrons have an energy distribution. An even broader neutron energy distribution, with neutron energies extending all the way to zero, could be obtained using a reaction leading to a three-body final state, such as 3H(t,2n)4He. The neutrons could also be produced by two ICF implosions; if the targets are filled with a DT mixture then they would primarily be 14.1 MeV neutrons with an isotropic angular distribution.

The neutrons produced by the two sources travel outward until they strike each other, and some neutrons scatter from each other. Elastically scattered neutrons that are traveling in the correct direction can travel down the length of the collimator to be detected by a neutron detector. The collimator ensures that neutrons coming directly from the neutron source cannot reach the detector, only those that originate in the region between the two sources, from *nn* scattering, can be viewed.

For the purpose of estimating the neutron count rate, the volume of space viewed by the collimator can be divided into volume elements. The distance from each source to the volume element will determine the velocity, and hence the energy, of the neutrons reaching the volume element and scattering at a given time. The number of scattered neutrons that are traveling in the correct direction to enter the detector can be determined. Moreover, since the scattered neutron energy can also be calculated, the time-of-flight (TOF) to the detector can be determined. Integrating over the allowed volume and time allows the TOF distribution to be calculated. In an actual experiment, by measuring the neutron TOF, the cross section as a function of outgoing energy, and hence center-of-mass (CM) energy can be measured all at once. This would allow the CM cross section to be extrapolated to zero energy, and the scattering length to be measured.

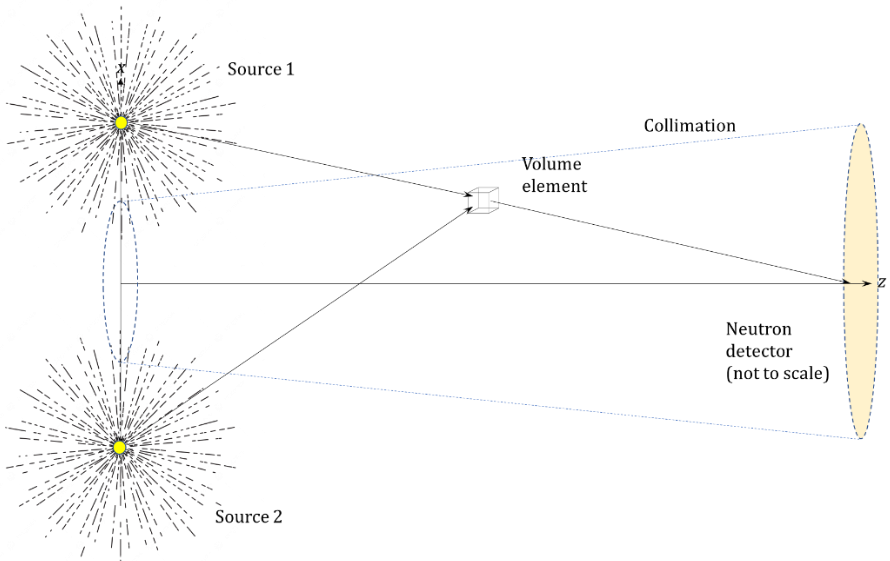

Figure 5. Simplified diagram of the proposed experiment. Simultaneous very short intense pulses of neutrons produced by ultrafast high-power lasers using ICF or TNSA travel outward from two sources and may elastically scatter from each other. A very long collimator ensures that neutrons directly from the sources cannot reach the neutron detector, but those that scatter off other neutrons inside the volume viewed by the collimator may do so.

IV. Neutron yields from TNSA ion energy distributions striking thick targets

In order to estimate the expected counts for the TNSA type of experiment, the first step is to calculate the time evolution of the neutron spectrum as a function of outgoing neutron energy and angle.

One technique is to use monoenergetic neutron producing nuclear reactions such as ^{2}H(d,n)^{3}He, ^{3}H(d,n)^{4}He, ^{7}Li(p,n)^{7}Be, ^{7}Li(d,n)^{8}Be and ^{12}C(d,n)^{13}N to produce an intense neutron field with a distribution of neutron energies when a thick target is bombarded with ions. If the incident ions themselves have an energy distribution, such as is the case with ions accelerated via Target Normal Sheath Acceleration (TNSA), this outgoing neutron spectrum becomes even broader. Furthermore, at low energies in the center-of-mass frame, the neutrons from these reactions are usually distributed roughly uniformly with angle, but this distribution becomes forward-peaked in the lab frame as the ion energy is increased, resulting in wide variations in the neutron flux with energy and angle.

Several codes currently exist to model the neutron spectra produced by charged particle induced nuclear reactions that could be produced using TNSA ions. For example, the venerable DROSG-2000 code [22] calculates neutron fluencies as a function of neutron angle for a moderately large number of reactions, but does not predict the neutron energy spectrum. The codes TARGET [23, 24] and NeuSDesc [25] will calculate neutron spectra as well as include other effects, such as peak broadening due to energy and angular straggling. Unfortunately, these codes only include a handful of the most common neutron producing reactions, although other reactions can be added by hand. For the most complete simulation of the neutron energy and angular distribution, a general-purpose transport code such as MCNPX [26] could be used, albeit with lengthy computation time. MCNPX would include most of the possible neutron-producing processes, such as particle evaporation and preequilibrium emission, other stripping and direct interactions, and even spallation. Unfortunately, none of these will generate the evolution of the neutron spectrum as a function of time, although this could be done manually by stitching together neutron spectra for monoenergetic ions generated by these codes.

As a starting point for modeling neutron-neutron scattering experiments using TNSA and ICF to generate the neutrons, a straightforward and comprehensible system capable of quickly generating rough estimates for neutron energy and angular distributions for a wide variety of easily added neutron producing reactions was desired, including their time evolution. A simple-to-understand dedicated code was developed, first using SMath Studio [27] which is now being converted to use the Cling c++ just-in-time (JIT) compiler with the ROOT analysis framework [28] for added computational speed.

Consider the case of a monoenergetic beam of ions striking perpendicular to a thick target, and causing a nuclear reaction to occur as shown in Figure 6. As the ions penetrate into the target they lose energy, so that by the time they reach distance *x* their energy is *E(x).*

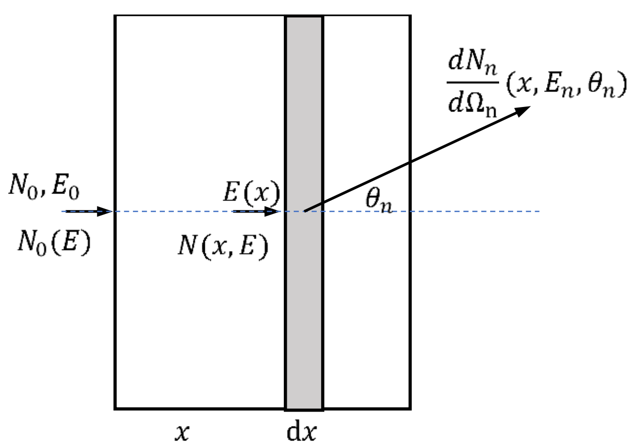

Figure 6. Ions striking a target lose energy as they penetrate. A number N_0 of incident monoenergetic ions with energy E_0 have energy *E(x)* after penetrating a distance *x* to a slice of thickness *dx*. In this slice, some ions cause nuclear reactions to occur, creating product nuclei and releasing $dN_n/d\Omega_n\,(x, E_n, \theta_n)$ neutrons at angle θ_n. A similar case occurs when the incident ions have a distribution of energies $N_0(E)$.

The thickness of the slice *dx* in which the ions lose energy *dE* will be

$$dx = \frac{1}{\frac{dE}{dx}(E)} dE \tag{5}$$

where dE/dx is the stopping power (negative value since the ions are losing energy) as a function of E. The range of the ions is therefore simply the distance the ions penetrate before they lose all of their energy

$$R = \int_{E_0}^{0} \frac{1}{\frac{dE}{dx}(E)} dE. \tag{6}$$

For monoenergetic ions, the number of reactions in each slice that emit a neutron into solid angle $d\Omega$ at angle θ_n is simply given by

$$\frac{dN_n}{d\Omega_\mathrm{n}}(x, \theta_n) = N_0 \frac{d\sigma}{d\Omega_\mathrm{n}}(E, \theta_n)\, \rho\, dx \tag{7}$$

where ρ is the number density of target nuclei and $\frac{d\sigma}{d\Omega_\mathrm{n}}(E, \theta_n)$ is the differential cross section. Integrating this over all the slices yields differential yield

$$\frac{dN_n}{d\Omega_\mathrm{n}}(\theta_n) = N_0 \rho \int_{E_0}^{0} \frac{\frac{d\sigma}{d\Omega_\mathrm{n}}(E, \theta_n)}{\frac{dE}{dx}(E)} dE \tag{8}$$

and the total yield is given by

$$N_n = 2\pi \int_{0}^{\pi} \frac{dN_n}{d\Omega_\mathrm{n}}(\theta_n)\, \sin\theta_n\, d\theta_n\,. \tag{9}$$

Finally, if the incident ion beam is not monoenergetic, this result can also be integrated over the incident ion energy spectrum $N_0(E)$ to obtain

$$\frac{dN_n}{d\Omega_\mathrm{n}}(\theta_n) = \int_{0}^{E_f} \rho N_0(E) \int_{E}^{0} \frac{\frac{d\sigma}{d\Omega_\mathrm{n}}(E', \theta_n)}{\frac{dE}{dx}(E')} dE' dE. \tag{10}$$

The integral in Equation (10) just gives the number of neutrons at a given angle, however, and does not provide the neutron energy distribution $Y(\theta_n, E_n) \equiv d^2N_n/dE_n d\Omega_n$. At each incident ion energy and scattering angle, the neutrons are emitted with a momentum- and energy-conserving corresponding neutron energy.

In order to include in the calculation the distribution of the outgoing neutron energies and angles, these integrals were performed numerically by slicing the target into thin sections in which the number, direction and energy of the scattered neutrons can be calculated. The outgoing neutron kinetic energy, $E_n(E_i,\ \theta_n)$, where θ_n is the laboratory neutron angle, was found for each slice using conservation of energy and momentum and is given for the non-relativistic case in Ref. [29]. The stopping power dE/dx was calculated for each particular ion and target using the code SRIM [30], and used to determine the incident ion energy loss in each slice. The neutron producing reaction laboratory cross sections were usually generated using DROSG-2000 Version 12.01 [22]. However, DROSG-2000 does not include many of the reactions of interest, and in some cases, such as ^{7}Li(d,n)^{8}Be, makes the unrealistic assumption that the cross section is isotropic. For reactions covered by DROSG, the predicted monoenergetic ion neutron spectrum can be compared to the results of the numerical calculation of Equation (10), as shown in Figure 7 and Figure 8.

This approach also would allow the time-evolution of the energy and angular distribution of the neutron flux, resulting from the incident TNSA ion time-of-flight, to be calculated, if desired. However, in the preliminary calculations this capability was not included since the width of the neutron pulse was short enough it was felt for the initial estimates it could be safety ignored. It can later be added by making use of the fact that the energy of the incident ion is a function of its velocity, and hence the arrival time of the ion at the neutron production target. That is, $N_0(E)$ can be recast as $N_0(t)$.

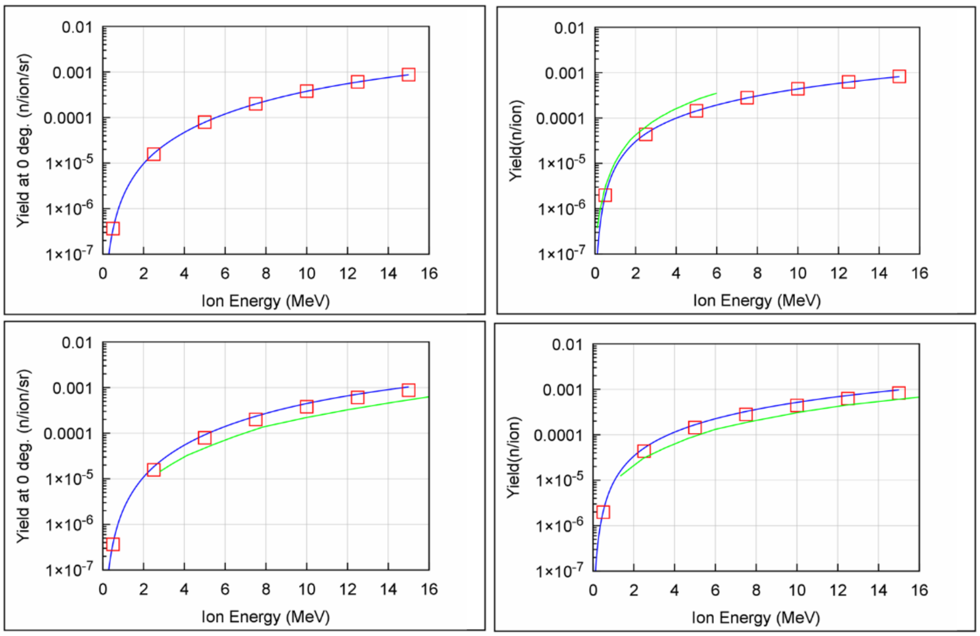

Figure 7. Computed monoenergetic ^{2}H(d,n)^{3}He total neutron yield (right column) and yield at at 0° (left column) as a function of deuteron energy for a D_2O ice (top row) and deuterated polyethylene (bottom row) target. Predicted yield (blue) is compared with prediction from DROSG-2000 (red squares) and Zuo et al. [31] (green).

Figure 9 compares the total predicted neutron yield for monoenergetic ions inducing the ^{2}H(d,n)^{3}He, ^{3}H(d,n)^{4}He, ^{7}Li(d,n)^{8}Be, and ^{7}Li(p,n0)^{7}Be reactions in thick targets as a function of ion energy. The TNSA process tends to produce an ion distribution that is highly peaked at low energies, so to maximize neutron production it might make sense to use a reaction like ^{3}H(d,n)^{4}He that maximizes neutron yield at low ion energies. Unfortunately, however, this reaction produces high energy (>14 MeV) neutrons -- for an *nn* scattering measurement low energy neutrons are desirable. A possible solution might be ^{3}H(t,2n)^{2}He [32], which has an energy threshold of 0 MeV, a relatively large cross section at low energies, and, because it has a three-body final state, the neutron energy spectrum reaches all the way down to zero.

In order to calculate the expected yield resulting from the ion energy spectrum produced by TNSA accelerated ions, the monoenergetic neutron yields were integrated over the ion spectrum. The TNSA ion pulse energy distribution was modeled using the formula

$$\frac{d^2N_d}{dE_d d\Omega_d}(E) = N_1 e^{-\mu_1 E} + N_2 e^{-\mu_2 (E-E\alpha)^2} + N_3 \tag{11}$$

with appropriate values for the coefficients selected to give rough agreement with the overall shape obtained from TNSA experiments, such as those described in Ref. [33,34]. Using this distribution, the expected timing shape of the ion pulse hitting the neutron production target (with solid angle $\Delta\Omega_d$) can be calculated. For example, as shown in Figure 10, for the ^{2}H(d,n)^{3}He reaction, using a 1 mm diameter solid deuterium neutron production target of and located 3 mm from the laser target, a FWHM time spread of only about 250 ps is expected.

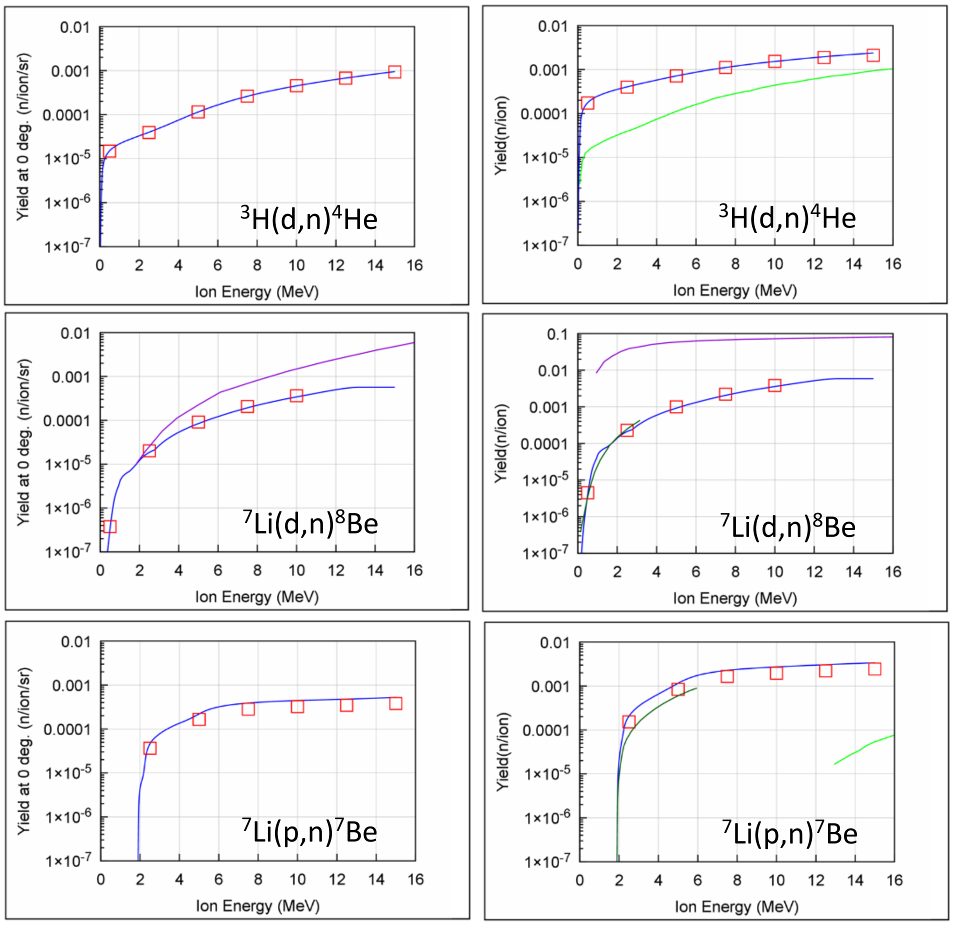

Figure 8. Computed monoenergetic neutron yield for ^{3}H(d,n)^{4}He with a solid tritium target (top row) and ^{7}Li(d,n)^{8}Be (middle row) and ^{7}Li(p,n0)^{7}Be (bottom row) with solid lithium targets. The total neutron yield (right column) and yield at 0° (left column) are plotted as a function of deuteron energy. Predicted yield (blue curve) is compared with prediction from DROSG-2000 (red squares), Zuo et al. [31] (dark green curve), Ke et al. [35], and Davis et al. [36] (purple), which includes other neutron producing reactions as well as ^{7}Li(d,n)^{8}Be.

Using the incident TNSA deuteron spectrum from Figure 10 the expected neutron yield as a function of neutron energy and angle can be calculated. The results for the ^{2}H(d,n)^{3}He reaction in a thick solid deuterium target are shown in Figure 11.

Although the time-dependence of the neutron yield could also be accounted for using the technique described in this paper, the approximation has been made to treat the neutrons as being emitted simultaneously, since, for the expected dimensions, the width of the neutron pulse is expected to be relatively short. For example, roughly using the measured OMEGA-EP TNSA energy spectrum for the incident deuterons and producing neutrons via ^{2}H(d,n)^{3}He in a thick deuterium target 3 mm from the laser target, the FWHM of the neutron pulse is expected to be about 0.25 ns, and by 1 ns over 95% of the neutrons will have been emitted. This assumption can be corrected later if necessary.

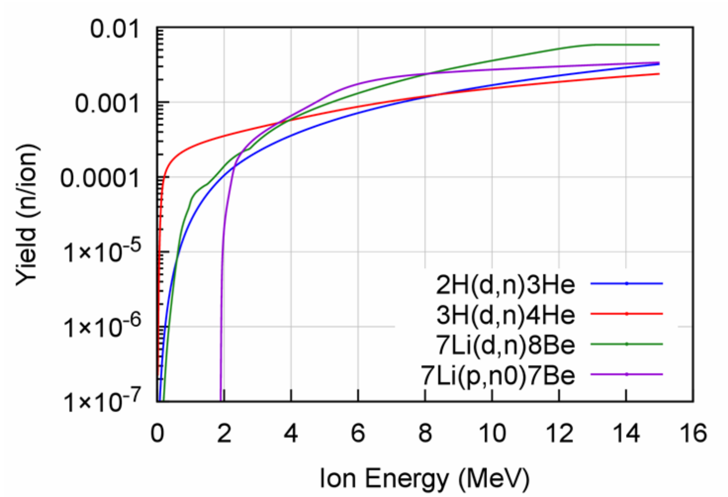

Figure 9. Comparison of predicted total monoenergetic neutron yields for ^{2}H(d,n)^{3}He in a thick solid deuterium target (blue), ^{3}H(d,n)^{4}He in a thick solid tritium target (red), ^{7}Li(d,n)^{8}Be in a thick natural lithium target (green) and ^{7}Li(p,n0)^{7}Be in a thick natural lithium target (purple).

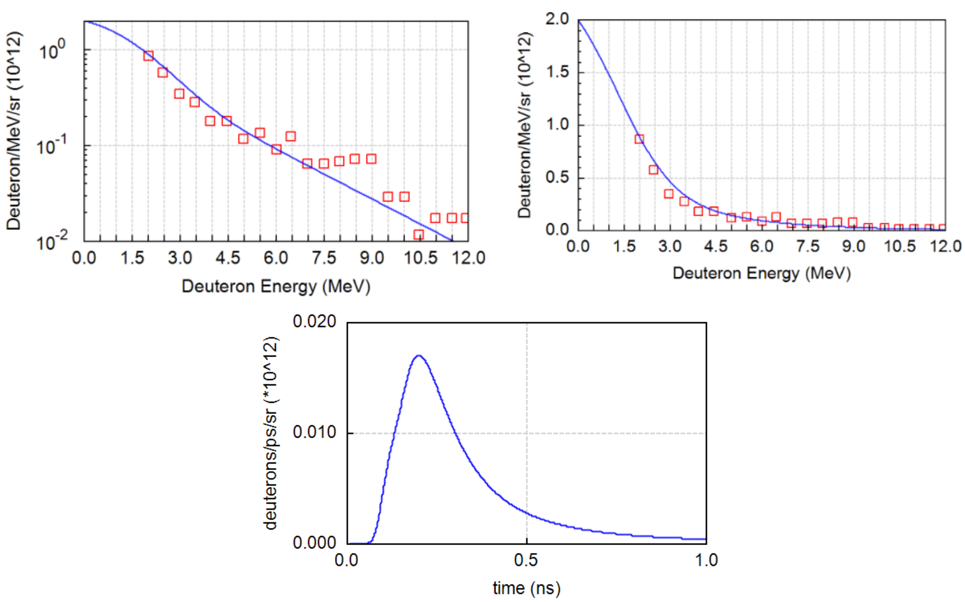

Figure 10. (Top) Approximate fit to the deuteron energy distribution using Equation (11) (blue) compared to measured distribution from Fig. 5.4 in Ref. [34] for a 663J $\cdot 10^{17}$ W/cm^2 OMEGA-EP laser shot (red) plotted with log (left) and linear (right) axes. The integrated number of deuterons from Equation (11) is 3.9×10^{11} compared with 2×10^{11} from Ref. [34]. (Bottom) The predicted time distribution for deuterons arriving at the neutron production target, a distance of 3 mm away.

V. *nn* Scattering Rate Calculation

The first step in determining the *nn* scattering rate is to calculate the neutron density field. Consider the volume element $dV = dA\, d\ell$ shown in Figure 12. If the neutrons are traveling with velocity $\vec{v}$ away from the source, then the rate of neutrons entering the volume element, dN_n/dt, will be

$$\frac{dN_n}{dt} = \frac{d^2N_n}{dt\, d\Omega_\mathrm{n}}\, d\Omega_\mathrm{n} = \frac{dN_n}{dt\, d\Omega_\mathrm{n}}\, \frac{dA}{r^2} \tag{12}$$

where $d^2N_n/dt\,d\Omega_n$, with units of s^{-1} sr^{-1}, is the rate neutrons cross dA where $d\Omega = dA/r^2$ is the solid angle. The amount of time required to cross the length $d\ell$ of the volume element will be $dt = d\ell/v$ so the density of neutrons ρ at a distance r from the source will be

$$\rho = \frac{dN_n}{dV} = \frac{dN_n}{dt}\frac{dt}{dV} = \frac{d^2N_n}{dt\,d\Omega_n}\frac{dA}{r^2}\frac{d\ell}{v\,dV} = \frac{d^2N_n}{dt\,d\Omega_n}\frac{1}{vr^2}. \tag{13}$$

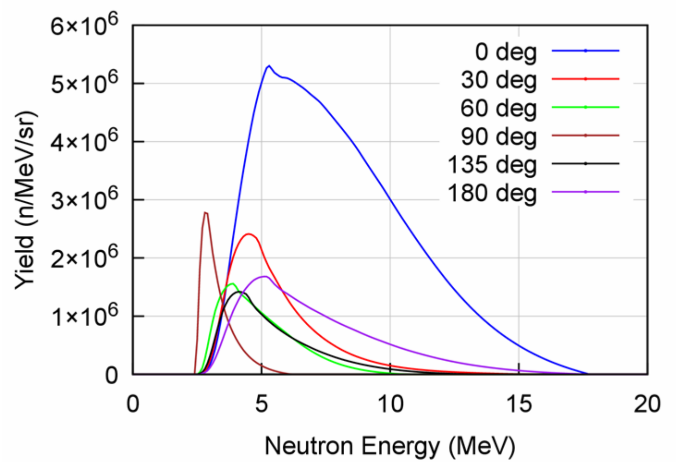

Figure 11. Neutron yield as a function of outgoing neutron energy at several angles produced by the ^{2}H(d,n)^{3}He in a thick solid deuterium target for the incident deuteron energy distribution shown in Figure 10.

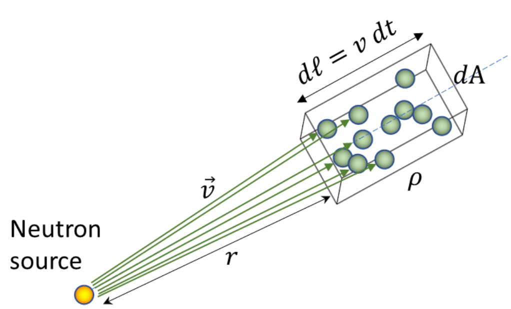

Figure 12. Neutrons emitted by the neutron source travel outward until they reach a small element of volume. The density of neutrons in the volume can be calculated as described in the text.

Neutrons from each source will strike each other and scatter. To calculate the number scattered, it is necessary to use the predicted *nn* scattering cross section from Equation (2) which is defined in the center-of-mass (CM) frame, as shown in Figure 13.

In order to convert this cross section to the laboratory frame, the laboratory coordinates ($\overrightarrow{x1}$ and $\overrightarrow{x2}$) and the center-of-mass coordinates ($\overrightarrow{x1}cm$ and $\overrightarrow{x2}cm$) are needed. Non- relativistically these are related by

$$\vec{x}cm = \frac{m_n\overrightarrow{x1} + m_n\overrightarrow{x2}}{m_n + m_n} = \frac{1}{2}(\overrightarrow{x1} + \overrightarrow{x2}), \tag{14}$$

$$\vec{x}rel = \overrightarrow{x1} - \overrightarrow{x2}, \tag{15}$$

$$\overrightarrow{x1}cm = \overrightarrow{x1} - \vec{x}cm, \text{ and} \tag{16}$$

$$\overrightarrow{x2}cm = \overrightarrow{x2} - \vec{x}cm \tag{17}$$

where m_n is the neutron mass. Taking the time derivatives yields the classical velocities in the two frames

$$\vec{v}cm = \frac{1}{2}\left(\overrightarrow{v1} + \overrightarrow{v2}\right), \tag{18}$$

$$\vec{v}rel = \overrightarrow{v1} - \overrightarrow{v2}, \tag{19}$$

$$\overrightarrow{v1}cm = \overrightarrow{v1} - \vec{v}cm = \frac{1}{2}\left(\overrightarrow{v1} - \overrightarrow{v2}\right) = \frac{1}{2}\vec{v}rel, \text{ and} \tag{20}$$

$$\overrightarrow{v2}cm = \overrightarrow{v2} - \vec{v}cm = -\frac{1}{2}\left(\overrightarrow{v1} - \overrightarrow{v2}\right) = -\frac{1}{2}\vec{v}rel. \tag{21}$$

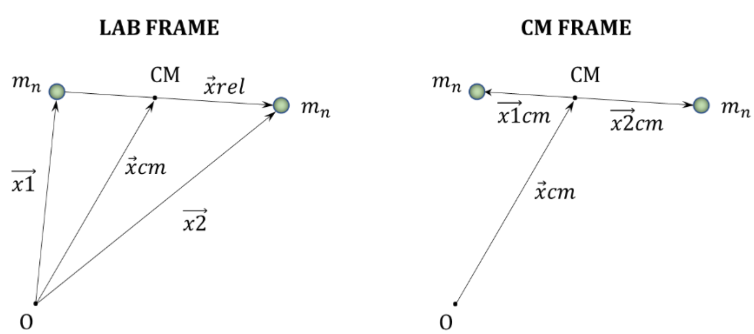

Figure 13. Two neutrons scattering in the laboratory (left) and center-of-mass (right) frames. The diagrams define the laboratory coordinates ($\overrightarrow{x1}$ and $\overrightarrow{x2}$) and the center-of-mass coordinates ($\overrightarrow{x1}$cm and $\overrightarrow{x2}$cm) for neutron-neutron scattering.

Now let's look at what happens in both the laboratory and CM frames when the neutrons from the two sources scatter off each other, as shown in Figure 14. Since Equations (14) to (21) are non-relativistic, the description below is only a good approximation for low neutron energies. However, even for energies as high as 50 MeV, the difference between the classical and relativistic velocities differ by only about 4%. For these energies it is also a good approximation to assume there is no time dilation and that the neutron densities ρ_1 and ρ_2 are not affected by length contraction and are therefore the same in both reference frames.

In this case, consider the collision of the neutrons in the two volume elements in Figure 14. The reaction rate dN_s/dt can be written terms of the luminosity $\mathcal{L}$ as

$$\frac{dN_s}{dt} = \mathcal{L}\,\sigma \tag{22}$$

where σ is the total cross section, which is the same in all inertial reference frames. The luminosity "integrated over" time dt, which is the time it takes the two volume elements to pass through each other, during which the collisions can occur, is

$$\mathcal{L}\,dt = \frac{N_1 N_2}{dA} \tag{23}$$

where N_1 and N_2 are the number of neutrons in each volume element, respectively, and dA is the area of the completely overlapping face of each volume element.

Now, since from Equations (20) and (21) the velocities in the CM frame must be equal and opposite, $\overrightarrow{v1cm} = -\overrightarrow{v2cm}$, the two volume elements are the same size ($dV = d\ell dA$) and the time required for the two elements to pass each other is $dt = d\ell/vrel$. The total number of reactions is therefore

$$dN_s = \frac{N_1 N_2}{dA}\sigma = \frac{\rho_1 dV\ \rho_2\ dV}{dA}\sigma = \rho_1\,\rho_2\ \ dV\ d\ell\ \sigma = \rho_1\,\rho_2\ \ dV\ d\ell\ \sigma = \rho_1\,\rho_2\ \ dV\ dt\ vrel\ \sigma \tag{24}$$

and so the rate of reactions for a given volume element is

$$\frac{d^2 N_s}{dt\ dV} = \rho_1\,\rho_2\ vrel\ \sigma \tag{25}$$

which agrees with Ref. [37] for average values and with the "colliding beams" case in Ref. [38] but disagrees by a factor of two with Ref. [16].

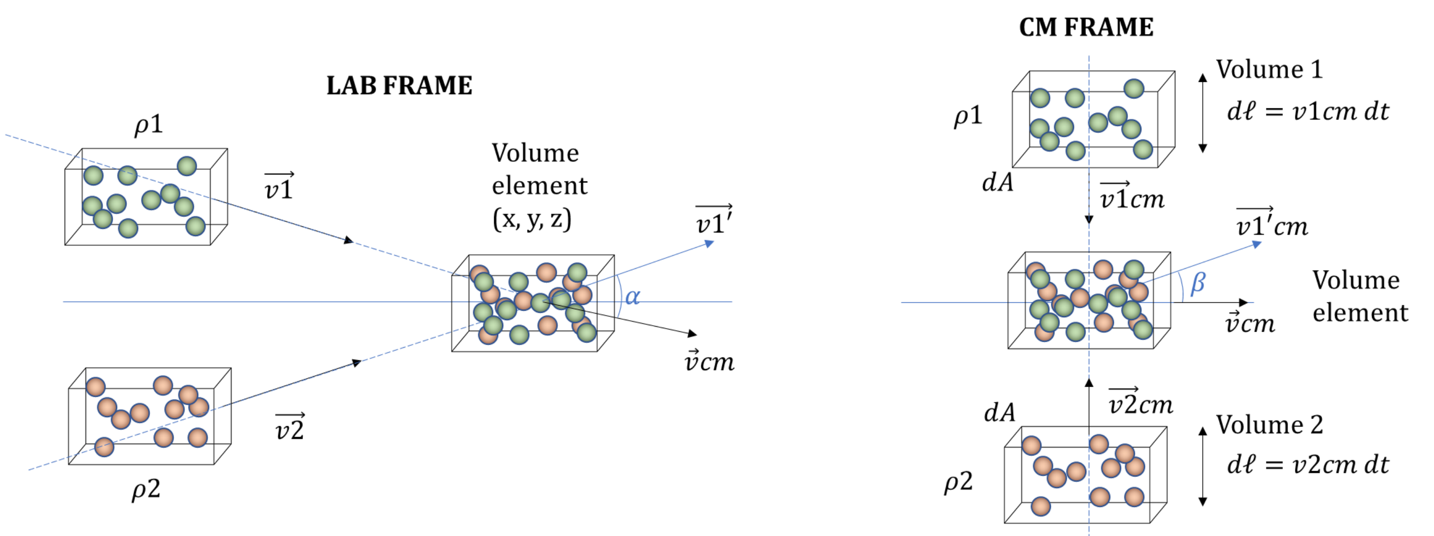

Figure 14. In the lab frame (left) neutrons from each source are traveling toward the volume element, where they can interact. The densities of the neutrons, ρ_1 and ρ_2, depend on the distance from each source according to Equation (13). In the CM frame (right) the neutrons have a head-on collision.

Notice that the luminosity is the same in every reference frame since it just depends on the number of neutrons in the volume element, and non-relativistically the density and size of the volume element is the same in every inertial frame. Therefore, the reaction rate is also the same in every reference frame since its just the product of the total cross section, which does not depend on the frame, and the luminosity. The differential cross section, however, does depend on the reference frame, so for scattering neutrons at a particular angle in the CM frame

$$\frac{d^3N_s}{dt\ dV\ d\Omega_{\text{cm}}} = \rho_1\ \rho_2\ vrel\ \frac{d\sigma}{d\Omega_{\text{cm}}} \tag{26}$$

which yields the number of neutrons into solid angle $d\Omega_{\text{cm}}$ in the CM frame by each volume element dV per unit time. This is not the same number as would be scattered at the corresponding angle in the laboratory frame, which would be

$$\frac{d^3N_s}{dt\ dV\ d\Omega_{\text{lab}}} = \rho_1\ \rho_2\ vrel\ \frac{d\sigma}{d\Omega_{\text{lab}}}. \tag{27}$$

By integrating over all space in the laboratory frame, the total number of neutrons scattered into the detector can be calculated as a function of time. However, to do this it is necessary to first determine $d\sigma/d\Omega_{\text{lab}}$ in terms of $d\sigma/d\Omega_{\text{cm}}$.

To determine this relationship the prescription of Amaldi [39] will be roughly followed. Consider the left side of Figure 15 which shows how the collision appears in the center of mass frame. In this figure, the primes indicate the quantity after the collision, absence of a prime indicates before the collision. Since both particles are neutrons both before and after the collision, and since $\overrightarrow{v1}cm = -\overrightarrow{v2}cm$, conservation of momentum gives

$$\overrightarrow{v1}cm + \overrightarrow{v2}cm = \overrightarrow{v1'}cm + \overrightarrow{v2'}cm = 0 \tag{28}$$

so

$$\overrightarrow{v1'}cm = -\overrightarrow{v2'}cm \tag{29}$$

and conservation of energy gives

$$v1cm^2 + v2cm^2 = v1cm'^2 + v2cm'^2 \tag{30}$$

so

$$|v1cm| = |v2cm| = |v1cm'| = |v2cm'|. \tag{31}$$

The speeds of all the neutrons are the same in the center of mass frame, both before and after the collision.

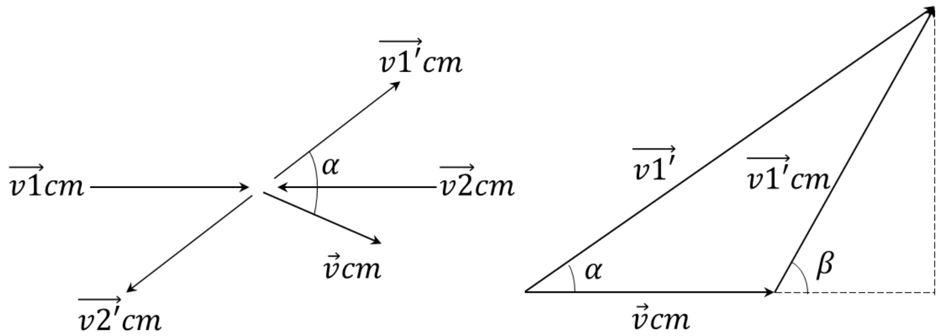

Figure 15. (Right) Velocities of incident ($\overrightarrow{v1}cm$ and $\overrightarrow{v2}cm$) and outgoing ($\overrightarrow{v1'}cm$ and $\overrightarrow{v2'}cm$) neutrons in the center-of-mass frame. (Left) Relationship from Equation (18) between $\overrightarrow{v1}cm$, $\overrightarrow{v1}$, and $\vec{v}cm$. The angles α and β are between the velocity of the center of mass $\vec{v}cm$ and the outgoing neutron in the laboratory and center of mass frames respectively.

Clearly, Equation (20) also holds true after the collision, so

$$\overrightarrow{v1'} = \overrightarrow{v1'}cm + \vec{v}cm \tag{32}$$

which is shown on the right side of Figure 15. The speed of the outgoing neutron in the laboratory frame $v1'$ can be obtained using the components in the direction of $\vec{v}cm$

$$v1' \cos\alpha = v1cm' \cos\beta + vcm \tag{33}$$

and perpendicular

$$v1' \sin\alpha = v1cm' \sin\beta \tag{34}$$

where β is the scattering angle in the CM frame (i.e. the angle between $\overrightarrow{v1'}cm$ and $\vec{v}cm$) and α is the corresponding laboratory angle (i.e. between $\overrightarrow{v1'}$ and $\vec{v}cm$). Eliminating β and using the quadratic formula gives the outgoing neutron speed

$$v1' = vcm\left[\cos\alpha \pm \sqrt{a^{-2} - \sin^2\alpha}\right] \tag{35}$$

where $a = 2vcm/vrel$. There are as many as two possible values for the outgoing laboratory speed, arising from the fact that there are two angle configurations for $\overrightarrow{v1'}cm$ with the same value for $\sin\beta$.

For a given α then, in general, it might be expected that there would be up to two possible allowed values of β. These can be calculated by substituting Equation (35) into Equation (34)

$$\sin\beta = a\sin\alpha\left[\cos\alpha \pm \sqrt{a^{-2} - \sin^2\alpha}\right] \tag{36}$$

and α can be found in terms of β by eliminating $v1'$ from Equations (33) and (34) to get

$$\tan\alpha = \frac{\sin\beta}{a + \cos\beta}. \tag{37}$$

From this, with a little algebra, the Jacobian for converting the differential cross section from the CM to the laboratory frame can be found since, in general, for axial symmetry $d\Omega = 2\pi \sin\theta \, d\theta = -2\pi \, d(\cos\theta)$ so

$$\frac{d\sigma}{d\Omega_{\mathrm{lab}}} = \frac{d\Omega_{\mathrm{cm}}}{d\Omega_{\mathrm{lab}}} \frac{d\sigma}{d\Omega_{\mathrm{cm}}} = \frac{d(\cos\beta)}{d(\cos\alpha)} \frac{d\sigma}{d\Omega_{\mathrm{cm}}} = \left| \frac{[\sin^2\beta + (a + \cos^2\beta)^2]^{\frac{3}{2}}}{1 + a\cos\beta} \right| \frac{d\sigma}{d\Omega_{\mathrm{cm}}} \tag{38}$$

which is the familiar result.

To determine these quantities, use the laboratory frame definitions in Figure 16. The position vector for Source 1 is $\overrightarrow{XS1}$, and for Source 2 is $\overrightarrow{XS2}$. Throughout the rest of this derivation only quantities for Source 1 will be explained, the extension to Source 2 and the numbering convention being obvious. The vector from each source to the "aim point" ($\overrightarrow{XSA1}$ and $\overrightarrow{XSA2}$), which is the point at which the vector normal to the center of the neutron production target intersects the z axis, is given by

$$\overrightarrow{XSA1} = \overrightarrow{XA} - \overrightarrow{XS1} \text{ and } \overrightarrow{XSA2} = \overrightarrow{XA} - \overrightarrow{XS2} \tag{39}$$

For the volume element located at $\overrightarrow{XE}$ with coordinates (x, y, z) then the vectors $\overrightarrow{XSE1}$ and $\overrightarrow{XSE2}$ from each source to the volume element are

$$\overrightarrow{XSE1} = \overrightarrow{XE} - \overrightarrow{XS1} \text{ and } \overrightarrow{XSE2} = \overrightarrow{XE} - \overrightarrow{XS2}. \tag{40}$$

The angles between the aim point and the volume element for each source are given by

$$\theta 1 = \cos^{-1} \frac{\overrightarrow{XSA1} \cdot \overrightarrow{XSE1}}{|\overrightarrow{XSA1}|\,|\overrightarrow{XSE1}|} \text{ and } \theta 2 = \cos^{-1} \frac{\overrightarrow{XSA2} \cdot \overrightarrow{XSE2}}{|\overrightarrow{XSA2}|\,|\overrightarrow{XSE2}|}, \tag{41}$$

where θ1 and θ2 are the angles of neutron emission in the neutron yield spectrum $Yn(\theta n, En)$, i.e. a neutron emission angle of 0° is directly toward the aim point. The vector from the volume element to the neutron detector is

$$\overrightarrow{XEN} = \overrightarrow{XN} - \overrightarrow{XE} \tag{42}$$

where $\overrightarrow{XN}$ is the position vector of the center of the neutron detector.

From these vectors the velocities and energies can be calculated at a given time t after the laser shot. The laboratory frame velocities of the incident neutrons in the volume element is

$$\overrightarrow{v1} = \frac{\overrightarrow{XSE1}}{t} \text{ and } \overrightarrow{v2} = \frac{\overrightarrow{XSE2}}{t}. \tag{43}$$

Equations (18) through (21) can then be applied to determine $\vec{v}cm$, $\vec{v}rel$, $\overrightarrow{v1}cm$ and $\overrightarrow{v2}cm$. The non-relativistic individual and relative kinetic energies are

$$E1 = \frac{1}{2} m_n \, v1^2, \; E2 = \frac{1}{2} m_n \, v2^2, \text{ and } Erel = \frac{1}{2} \mu \, vrel^2 \tag{44}$$

where μ is the reduced mass $\mu = m_n/2$. The laboratory scattering angle α between $\overrightarrow{v1'}$ and $\vec{v}cm$ is

$$\alpha = \cos^{-1}\left(\frac{\overrightarrow{XEN}\cdot\vec{v}cm}{|\overrightarrow{XEN}||\vec{v}cm|}\right). \tag{45}$$

and so the two possible values of the magnitude of the outgoing neutron velocity $\overrightarrow{v1'}$ are given by Equation (35) and the corresponding the CM scattering angles $\beta 1$ and $\beta 2$ between $\overrightarrow{v1'cm}$ and $\vec{v}cm$ are given by Equation (36), as shown in Figure 17.

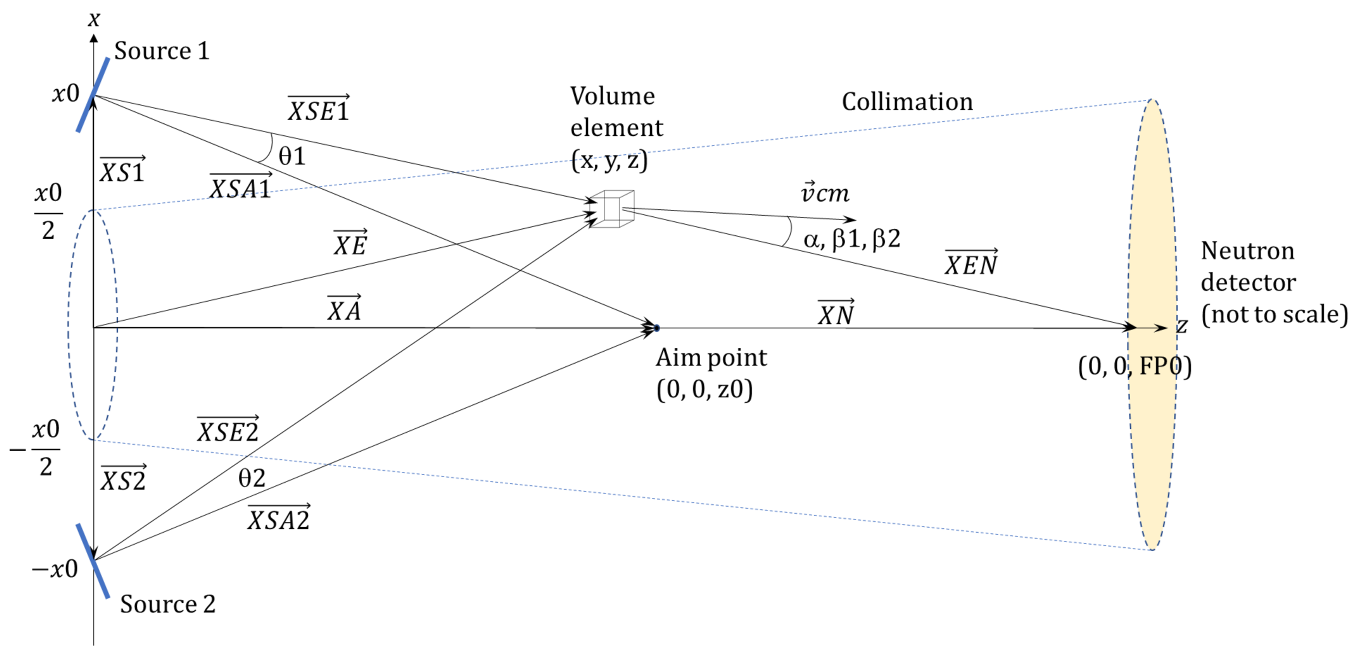

Figure 16. Neutrons produced by two sources have an energy and angular distribution $Y(\theta_n, E_n) \equiv d^2N_n/dE_n d\Omega_n$ that varies with time, resulting in the neutrons scattering from each other in the volume surrounding the sources. A collimator restricts the volume from which scattered neutrons can reach the neutron detector and be counted. This volume is divided into tiny volume elements in which the total number of nn interactions and the number of neutrons scattered into the detector can be calculate for each short time interval. The vectors used in the calculation are defined in this diagram, which is not to scale. In particular, the distance to the neutron detector (FP0) should be much larger than shown relative to the other dimensions.

The neutron densities from each source at the volume element are given by Equation (13), that is

$$\rho 1 = \frac{\frac{d^2N_n}{dE1 d\Omega_n}\frac{dE1}{dt}}{\left|\overrightarrow{XSE1}\right|^2 |\overrightarrow{v1}|} = \frac{Y(\theta 1, E1)}{\left|\overrightarrow{XSE1}\right|^2 |\overrightarrow{v1}|}\frac{dE1}{dt} \text{ and } \rho 2 = \frac{\frac{d^2N_n}{dE2 d\Omega_n}\frac{dE2}{dt}}{\left|\overrightarrow{XSE1}\right|^2 |\overrightarrow{v1}|} = \frac{Y(\theta 2, E2)}{\left|\overrightarrow{XSE1}\right|^2 |\overrightarrow{v1}|}\frac{dE2}{dt} \tag{46}$$

where

$$\frac{dE1}{dt} = \frac{m_n\left|\overrightarrow{XSE1}\right|^2}{t^3} \text{ and } \frac{dE2}{dt} = \frac{m_n\left|\overrightarrow{XSE2}\right|^2}{t^3}. \tag{47}$$

The laboratory cross sections are given by Equations (2), (50) and (38).

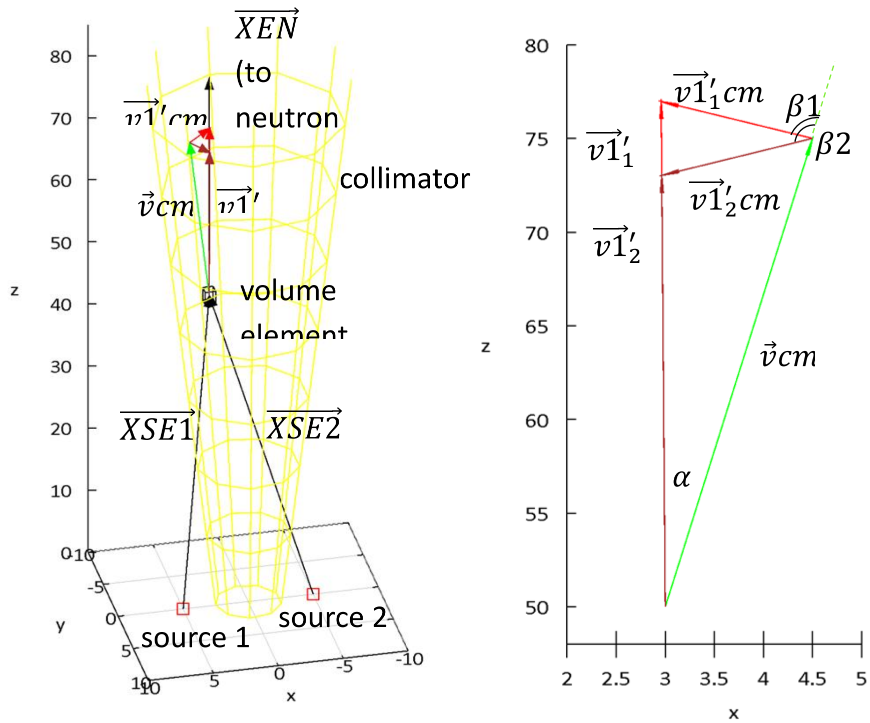

Figure 17. (Left) Geometry generated by the SMath code showing $\vec{v}cm$, $\overrightarrow{v1'}$, and $\overrightarrow{v1'}cm$ for a particular volume element. (Right) Zoomed in view. The angle α is determined by requiring $\overrightarrow{v1'}$, the velocity of the outgoing neutron in the lab, to point toward the neutron detector using Equation (45). From this, the two possible magnitudes of $\overrightarrow{v1'}$ are determined using Equation (35), corresponding to the two possible values of β obtained from Equation (36).

This is everything that is needed to integrate Equations (25) and (27) over all the volume that can be viewed by the neutron detector restricted by the collimator, so that the total number of neutrons scattered will be

$$N = \int_t \int_V \frac{d^2 N_s}{dt\, dV} dV\, dt = \int_t \int_V \rho_1 \rho_2\, vrel\, \sigma\, dV\, dt \,.. \tag{48}$$

and the number scattered into the detector will be

$$Ndet = \int_t \int_V \frac{d^3 N_s}{dt\, dV\, d\Omega_{\text{lab}}} dV\, dt = \int_t \int_V \rho_1 \rho_2\, vrel\, \frac{d\sigma}{d\Omega_{\text{lab}}}\, dV\, dt\, \Delta\Omega. \tag{49}$$

where $\Delta\Omega$ is the (small) solid angle of the neutron detector. Note that this integral is somewhat tricky to perform since neutrons scattered at two different angles in the CM frame will have the correct angle in the lab frame to enter the detector. In practice, this was accounted for by adding both contributions to the total number detected for those volume elements and times.

VI. Results and future improvements

SMath was originally chosen to implement this calculation because it made development and testing of these calculations easy, not because of its speed. Because it is so slow, even when optimized for numerical calculations, only a single calculation has been carried out in its entirety so far – using the TNSA deuteron spectra from OMEGA-EP from Figure 10 striking a thick solid deuterium target to produce the neutron spectra shown in Figure 11. The solid deuterium neutron production targets were 5 mm apart and aimed at a point along the centerline 5 cm from the origin. The 12.7 cm (5 inch) radius neutron detector was 2 m away along the centerline. The collimator was a truncated cone with radius 2.5 mm between the neutron sources, and 12.7 cm at the neutron detector.

The result using the physical dimensions above, reflection symmetry across the xz and yz planes to reduce computation time, and 45 volume elements with 0.8 ns time steps is that the total number of neutron scattering events per laser shot inside the collimator is 6.5×10^{-13} and the number detected by the detector is 1.4×10^{-13}. The TOF structure of the neutrons hitting the detector is shown in Figure 18. By using this TOF information it should be possible to reconstruct the energy dependence of the cross section, which would allow the extrapolation of the cross section to zero energy and the extraction of the scattering length.

Clearly, these numbers are many orders of magnitude lower than they would need to be to make a measurement of the scattering length. However, there are a number of strategies that can be employed to dramatically increase the yield, which are addressed below.

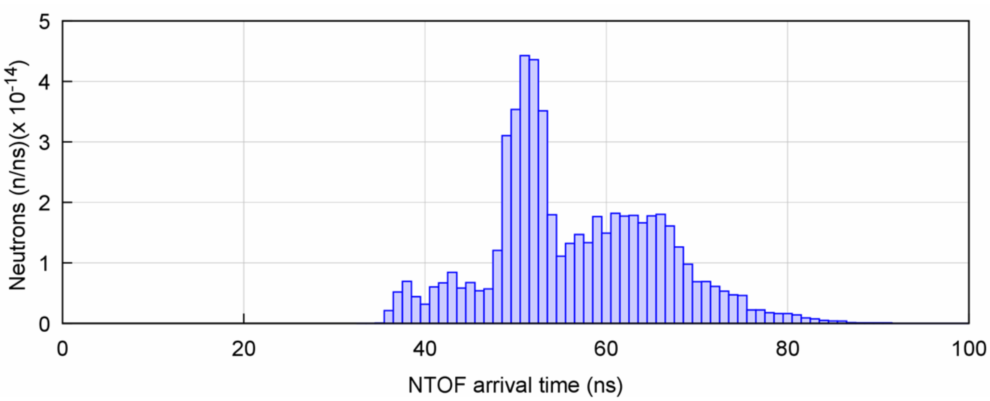

Figure 18. The predicted TOF spectrum for the neutrons reaching the detector. The structure is due to the complicated convolution of the neutron energy spectra and the changing conical distribution of the outgoing neutrons described in Section VI.C.

A. Higher laser power and a better neutron producing reaction

The most obvious way to improve the yield of scattered neutrons is to increase the laser power. In the calculation above, an especially low power density OMEGA-EP shot was used, the 663J, 10 ps pulse had a spot size of 300 μm has a power density of about 10^{20} W/m^2. A 1250 J, 10ps OMEGA-EP shot 30 μm in diameter has power density 2×10^{23} W/m^2. For an expected NSF-OPAL laser shot with 500 J in 20 fs with a beam spot of 2.3 μm radius, the power density would be 6×10^{27} W/m^2, an increase of 6×10^6. While the scale does not go down to such low intensities, Figure 19 shows the results of a simulation for d-d and d-Li neutron production for laser intensities similar to NSF-OPAL. By means of comparison, for the OMEGA-EP calculation in this paper the total neutron yield was 6×10^7 for 10^{20} W/m^2, higher than expected from Figure 19. Extrapolating from 10^{20} W/m^2 to 10^{27} W/m^2, it is not unreasonable to expect a factor of 10^3 increase in neutron yield, rising to 10^5 if the reaction is changed from d-d to d-Li. Since the number of scattered neutrons goes as the neutron density squared, this could immediately increase the neutron yield by a factor of 10^{10}, leaving only about a factor of 10^6 needed before such an experiment becomes doable. In the worst-case scenario, it could be imagined this factor of 10^6 would come from repetitions using NSF-OPAL.

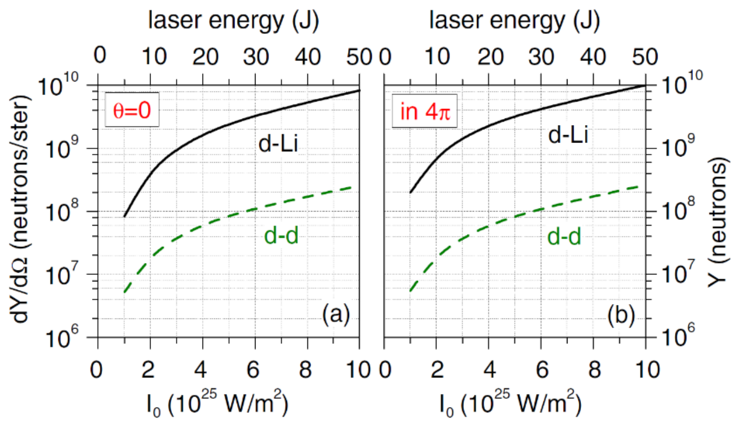

Figure 19. Simulated ^{7}Li(d,xn) neutron production by a well collimated deuteron beam generated using a high-intensity ultrashort pulse laser similar to NSF-OPAL, with $(1-5) \times 10^{25}$ W/m^2 in a 40 fs pulse with a beam spot of 2 μm. Neutron yield from d–Li (black solid line) and d–d (green dashed line) nuclear reactions in (a) the forward direction and (b) total neutron yield versus peak laser intensity/energy. Figure taken from Ref. [40].

In this analysis, the increase in neutron yield arises to a large extent because the incident deuteron pulse extends to higher energies for the high-power short-pulse laser pulse. This means the deuterons penetrate the target further, releasing more neutrons and higher energy along their path. These higher energy neutrons are more forward directed, so that more of them will collide, but will need to collide at a shallower angle for the relative energy to be low for a large scattering cross section. At these higher energies, many neutron producing reaction can occur, which also increases the neutron yield.

B. Use ^{3}H(d,2n)^{4}He to produce low energy neutrons?

Another idea would be to use a reaction producing low energy neutrons, like ^{3}H(d,2n)^{4}He (Figure 20). This would allow the “aim point” to be much closer to the neutron production targets and still have low-energy neutrons, thereby greatly increasing the neutron density in the collision region. This is much different than the case of the ^{7}Li(d,xn) reaction, in which the neutron yield was increased by increasing the deuteron energy and therefore also the outgoing neutron energy. Although this increases the yield, it also has the undesired effect of also increasing the average outgoing neutron energy. This is a problem because we are interested in measuring the cross section for low relative energies and, as is shown in Figure 1, the cross section falls rapidly with increasing neutron energy. In order to overcome this would require a very small “beam crossing” angle, that is, the “aim point” would need to be further away resulting in lower neutron densities than if the crossing point was closer to the neutron production targets. This problem is somewhat ameliorated by the fact that at high energies the neutrons are more forward focused.

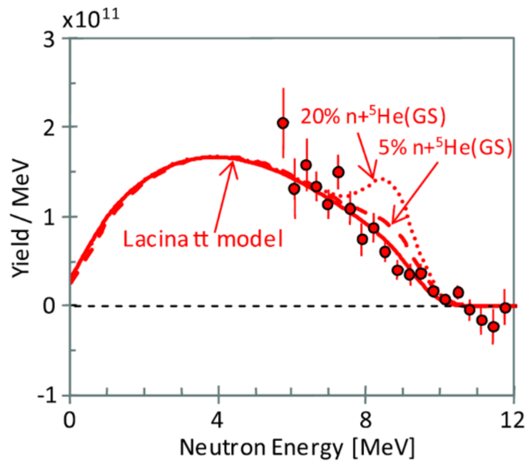

Figure 20. Measured (circles) and predicted tt neutron spectrum for gas-filled DT implosion at the OMEGA laser, showing predicted contributions for $n + n$+^{4}He channel (solid curve) and 5% and 20% contributions of n+^{5}He(gs) (dashed and dotted curves, respectively). The expected neutron yield extends all the way down to 0 MeV. Figure taken from Ref. [41].

C. Slice the detector into area elements in the simulation

In the simulation as it is currently constructed, the number of scattered neutrons/sr in the direction of the center of the detector is calculated, multiplied by the detector solid angle, and summed over all of the volume elements where the neutrons can scatter. This obviously assumes that variation of scattered neutrons with angle varies only slowly with angle. In fact, that is not true.

The low-energy cross section from Equation (2) is distributed isotropically in the CM frame, so that

$$\frac{d\sigma}{d\Omega_{\rm cm}}(\theta_{\rm cm}) = \frac{\sigma(k)}{4\pi}. \tag{50}$$

To convert the cross section from the CM to the laboratory frame, the Jacobian $d\Omega_{\rm cm}/d\Omega_{\rm lab}$ from Equation (38) can be used

$$\frac{d\sigma}{d\Omega_{\rm lab}} = \frac{d\Omega_{\rm cm}}{d\Omega_{\rm lab}}\frac{d\sigma}{d\Omega_{\rm cm}} \tag{51}$$

as well as the kinematic relationships to convert the angle in the CM frame to the laboratory frame from Equations (36) and (37). As shown in Figure 21 this converts the uniform CM distribution to one that is highly peaked in a cone surrounding the CM velocity of the incident *nn* pair.

This laboratory cross section distribution has immediate consequences for experiments like the one being proposed that measure the *nn* cross section at low relative energies by scattering two higher energy neutrons at a very shallow angle. Because the cross section is so highly peaked, the neutron rate at certain angles is much higher than at the center of the detector ($\sim 0°$), an effect that becomes more pronounced the lower the relative energy relative to the CM energy. Accounting for this by slicing the detector into area elements could greatly increase the simulated yield (thereby making it correspond to the actual yield in a real experiment), since the simulation is missing these angles.

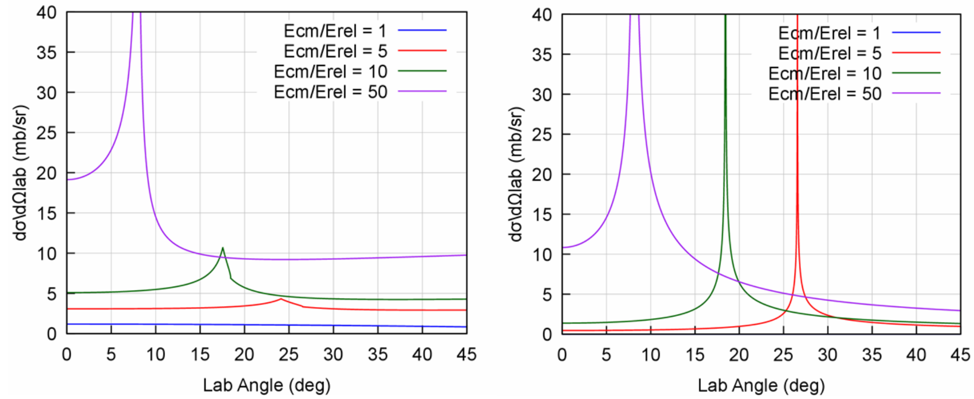

Figure 21. The *nn* elastic scattering cross section in the laboratory frame as a function of laboratory scattering angle α, which is defined to be the angle between the outgoing neutron and the laboratory velocity of the center of mass of the *nn* pair. The cross section was computed for the case of $Erel = 100$ keV for the ratio $Ecm/Erel = 1$ (blue), 5 (red), 10 (green) and 50 (purple) for the two allowed outgoing neutron lab velocities in Equation (35) corresponding to the two allowed CM angles $\beta 1$ (left) and $\beta 2$ (right) from Equation (36) that result in the same lab scattering angle α. For large CM velocity the cross section is highly peaked in a cone around the CM velocity vector.

VII. Future Plans

At the present time we have an SMath simulation code that seems to function correctly, but is too slow to carry out a program of exploring the parameter space for possible ways to measure the *nn* scattering length. We have begun the process of converting it to c++, and in the coming months hope to use the resulting faster simulation with smaller volume elements in the following ways:

1. Divide NTOF detector into area elements to better capture forward scattered “neutron cone”.
2. Use realistic OPAL TNSA deuteron spectra which should have significant strength at much higher energies.
3. Use the ^{7}Li(d,xn) cross sections from the JENDL/DEU-2020 deuteron neutron production library with our neutron source code and compare the resulting neutron spectra with MCNPX. Then use these to simulate *nn* scattering. Explore parameter space for OPAL-like *nn* measurement.
4. Use MCNPX to generate outgoing neutron spectra for ^{3}H(d,2n)^{4}He, then use these to simulate *nn* scattering. Explore parameter space for OPAL-like *nn* measurement.

This material is based upon work supported by the Department of Energy [National Nuclear Security Administration] University of Rochester “National Inertial Confinement Program” under Award Number(s) DE-NA0004144.

[1] Chad Forrest, "Neutron-Neutron Scattering with Two High Shot-Rate Neutral Beams," Appendix A8 in *OPAL – Optical Parameter Amplifier Line Flagship Experiment Selection Report*, S-OP-M-006 Rev A, August 2024 (unpublished).

[2] OPAL – Optical Parameter Amplifier Line Flagship Experiment Selection Report, S-OP-M-006 Rev A, August 2024 (unpublished), p.34.

[3] J. M. Blatt and V. F. Weisskopf, "Theoretical Nuclear Physics," John Wiley and Sons, New York, 1952.

[4] Ivo Šlaus, Yoshinori Akaishi, and Hajime Tanaka, Physics Reports **173**, 257-300 (1989).

[5] G A Miller, B M K Nefkens and I Slaus, Phys. Rep. 194, 1 (1990).

[6] V.A. Babenko and N.M. Petrov, "Determination of low-energy parameters of neutron-proton scattering on the basis of modern experimental data from partial-wave analyses," Phys. Atom. Nuclei **70**, 669–675 (2007). https://doi.org/10.1134/S1063778807040072

[7] C.R. Howell, "Review of Indirect Methods Used to Determine the Neutron-Neutron Scattering Length," Proceedings of the X International Seminar on Interactions of Neutrons with Nuclei, Dubna, Russia, ISINN-10 (2003), p. 71.

[8] G. A. Miller and W. T. H. Van Oers "Charge Independence and Charge Symmetry," Symmetries and Fundamental Interactions in Nuclei. (Canada & Canada 1995)), pp. 127-167.

[9] Y. Pokotilovski and G. Takhtamyshev, "Neutron-neutron scattering: Possibility of in-beam experiment," Phys. At. Nucl. **56**, 524 (1993).

[10] A. V. Dementiev et al, "On the possibility of direct investigations of neutron-neutron scattering at LHC beam dump". Proceeding of the 15th Meeting of the International Collaboration on Advanced Neutron Sources (ICANS-XV) (2001), p. 1019–1025.

[11] D. W. Glasgow et al. 'The Los Alamos National Laboratory Neutron-Neutron Scattering Program," Radiation Effects **94**, 239–243 (1986).

[12] W. I. Furman et al, J. Phys. G: Nucl. Part. Phys. **28,** 2627 (2002).

[13] E. I. Sharapov, et al, "Direct Measurement of Neutron-Neutron Scattering," AIP Conf. Proc. **680**, 261–264 (2003);.

[14] B. E. Crawford et al, J. Phys. G: Nucl. Part. Phys. **30,** 1269 (2004).

[15] G. E. MitchellI et al, "A direct measurement of the neutron-neutron scattering length," Braz. J. Phys. **35**, 850 (2005).

[16] E. I. Sharapov et al., in Proceedings of the 13th International Seminar on Interaction of Neutrons with Nuclei (ISINN 13), Dubna, Russian Federation, 25-28 May 2005, p. 130-136.

[17] G.E. Mitchell et al, J. Res. Natl. Inst. Stand. Technol. **110** , 225-230 (2005).

[18] A.Yu. Muzichka et al, "Background determination for the neutron–neutron scattering experiment at the reactor YAGUAR," Nuclear Physics A **789**, 30-45 (2007).

[19] W.I. Furman et al, AIP Conf. Proc. **1109**, 53–58 (2009).

[20] V.K. Ignatovich, "Analytical calculation of the neutron spectrum for direct measurement of NN scattering at pulsed reactor Yaguar," Phys. Atom. Nuclei **72**, 41–46 (2009).

[21] S.L. Stephenson et al, "Experiment on direct nn scattering - The radiation-induced outgassing complication," Nuclear Physics A 895, 33-43 (2012).

[22] M. Drosg, "DROSG-2000: Neutron source reactions. Data files with computer codes for 56 monoenergetic neutron source reactions.," IAEA-NDS-87(rev.5), (2000).

[23] D. Schlegel-Bickman, G. Dietze, and H. Schölermann, Nucl. Instr. And Meth. **169**. 517-526 (1980).

[24] Dietrich Schlegel, "TARGET user's manual", Laborbericht PTB-6.42-05-2, Braunschweig (2005).

[25] Birgersson E, Loevestam G. NeuSDesc-Neutron Source Description Software Manual. EUR 23794 EN. Luxembourg (Luxembourg): OPOCE; 2009. JRC51437.

[26] J. A. Kulesza, et al, MCNP Code Version 6.3.0 Theory & User Manual. Los Alamos National Laboratory Tech. Rep. LA-UR-22-30006, Rev. 1. Los Alamos, NM, USA. September 2022; D. B. Pelowitz, et al. MCNPXTM User's Manual, Version 2.7.0. Los Alamos National Laboratory Tech. Rep. LA-CP-11-00438. Los Alamos, NM, USA. April 2011.

[27] SMath Studio, https://smath.com/en-US/ (Accessed Nov. 12, 2024).

[28] Rene Brun and Fons Rademakers, ROOT - An Object Oriented Data Analysis Framework, Proceedings AIHENP'96 Workshop, Lausanne, Sep. 1996, Nucl. Inst. & Meth. in Phys. Res. A **389,** 81-87 (1997).

[29] A.S. Langsdorf, J.E. Monahan Jr. and W.A. Reardon, "A Tabulation of Neutron Energies from Monoenergetic Protons on Lithium", ANL-5219 (1954)

[30] J.F. Ziegler, J.P. Biersack, and M. Ziegler, "SRIM – The stopping and range of ions in matter," NIM **B268**, 1818-1823 (2010).

[31] Yubin Zuo, Guoyou Tang, Zhiyu Guo, Jimei Guo, Yuyang Pei, Jianguo Xu, Hu Wang, and Yuanong Lu, Physics Procedia 60, 220 – 227(2014).

[32] Göran Ericsson, Journal of Fusion Energy **38**, 330-355 (2019).

[33] A.K. Schwemmlein, C. Stoeckl, C.J. Forrest, W.T. Shmayda, S.P. Regan, W. U. Schröder, NIM B 522, 27 (2022).

[34] A. Schwemmlein, Ph. D. thesis, (University of Rochester, 2021).

[35] Jianlin Ke, Chunlei Wu, Meng Liu, Wei Ma, Xiaohai He, Benchao Lou, Yonghong Hu, Penghui Gao, Yan Li, Qinlong Zhang, Jun Tang, Yuanrong Lu, and Zhihui Li, NIM A 997, 165165 (2021).

[36] J. Davis, G M Petrov, Tz. Petrova, L. Willingale, A. Maksimchuk and K. Krushelnick, Plasma Phys. Control. Fusion **52,** 045015 (2010).

[37] B. E. Crawford et al., J. Phys. G: Nucl. Part. Phys. **30**, 1269-1285 (2004).

[38] Yu. N. Pokotilovski and G, G, Takhtamyshev, JINR-Report E3-92-417 (1992).

[39] E. Amaldi and S. Flügge (ed), Handbuch der Physik XXXVII/2 (Springer, Berlin, 1959), pp. 90-101..

[40] J. Davis et al, Plasma Phys. Control. Fusion **52**, 045015 (2010).

[41] D.T. Casey et al., Phys. Rev. Lett. **109**, 025003 (2012).